ISSN 0036-0295, Russian Metallurgy (Metally), Vol. 2016, No. 5, pp. 443–449. © Pleiades Publishing, Ltd., 2016.
Original Russian Text © D.A. Vasil'ev, A.L. Udovskii, 2016, published in Metally, 2016, No. 3, pp. 53–60.

Application of Physical–Empirical Models to Calculate a Fragment of the Phase Diagram and the Physical Properties of bcc Fe–Cr Alloys: II. Calculation of Phase Boundaries, Spinodal, and the Temperature Dependence of the Heat Capacity of an Alloy

D. A. Vasil'ev[a, *] and A. L. Udovskii[a, b, **]

[a] *Baikov Institute of Metallurgy and Materials Science, Russian Academy of Sciences, Leninskii pr. 49, Moscow, 119991 Russia*

[b] *National Research Nuclear University MEPhI, Kashirskoye sh. 31, Moscow, 115409 Russia*

*e-mail: *vasilyev-d@yandex.ru, **udovsky@imet.ac.ru*

Received October 14, 2015

Abstract—The contributions at a temperature of 500 and 600 K of the chemical, elastic, vibrational, magnetic, electronic, and configurational energies to the Gibbs energy of mixing of bcc alloys without regard for the contribution of a short-range order are calculated as functions of composition and temperature using physical–empirical models. The temperature dependences of the heat capacity of an alloy in both one- and two-phase states are calculated. The heat capacity jumps calculated for alloys of various compositions can be used to estimate the equilibrium solubility boundaries of Fe–Cr alloys, which can hardly be found from experimental data because of the slow diffusion processes that occur when an equilibrium state is reached. The calculated solubility boundary of bcc solid solutions and the spinodal and the heat capacity of Fe–Cr alloys are compared with the experimental data and the calculation results obtained in other works. The agreement and discrepancy between these data are discussed.

DOI: 10.1134/S003602951605013X

INTRODUCTION

This work is a continuation of work [1] on the application of physical–empirical models to estimate the contributions to the Gibbs energy of mixing of the ferromagnetic bcc solid solutions in the Fe–Cr system. The Fe–Cr system is the basis for creating ferritic corrosion-resistant steels due to the presence of chromium in an iron-based solid solution. Moreover, a thin chromium oxide film, which prevents further oxidation, is known to form on the surface of an Fe–Cr alloy under the action of an aggressive surrounding medium. When the chromium content in the alloy reaches ~10 at %, the corrosion resistance of ferritic steels increases by several orders of magnitude [2]. bcc Fe–Cr alloys are model alloys for creating that materials that have a high corrosion and radiation resistance and can operate at high temperatures of about 1000 K, which is the temperature at which next-generation reactors (fast reactors) should operate. These alloys can also be used as first-wall materials in the next-generation thermonuclear reactor.

Moreover, the addition of chromium to an iron matrix strongly changes the mechanical properties of iron-based alloy, the swelling and creep resistance, and the formation of radiation-induced pores. It is important that most physical (Curie temperature, Debye temperature, average magnetic moment), structural (short-range order [3, 4]), chemical (change in the sign of enthalpy of mixing [5–9]), and mechanical (bulk modulus [8]) properties of bcc Fe–Cr alloys are characterized by nonmonotonic behavior when the chromium concentration changes: they reach their extrema at a chromium concentration of about 10 at %.

Although the Fe–Cr system is based on a bcc structure over the entire concentration range, it contain alloys in stable and metastable (for a rather long time) states. In the temperature range 273–573 K, the estimated experimental Fe–Cr phase diagram [10] exhibits boundaries of solubility of chromium atoms in an iron matrix beginning from 5–10 and ending in 90–95 at % Cr. The following two ranges are present inside this region: two ranges of a metastable state of alloys, where $\partial^2 G/\partial x^2 > 0$, and one range of absolute instability (spinodal decomposition), where $\partial^2 G/\partial x^2 < 0$ (G is the Gibbs energy and x is the mole concentration of the second component). The first two ranges are located along the edges of the second range and extend through 20 at % on either side. The decomposition of alloys in the second range occurs according to the spinodal mechanism. Since this range has no thermodynamic barriers, the decomposition of alloys is a purely diffusion process. Note that the boundaries of spinodal decomposition are important from a practical viewpoint: knowing these boundaries, researchers can create materials

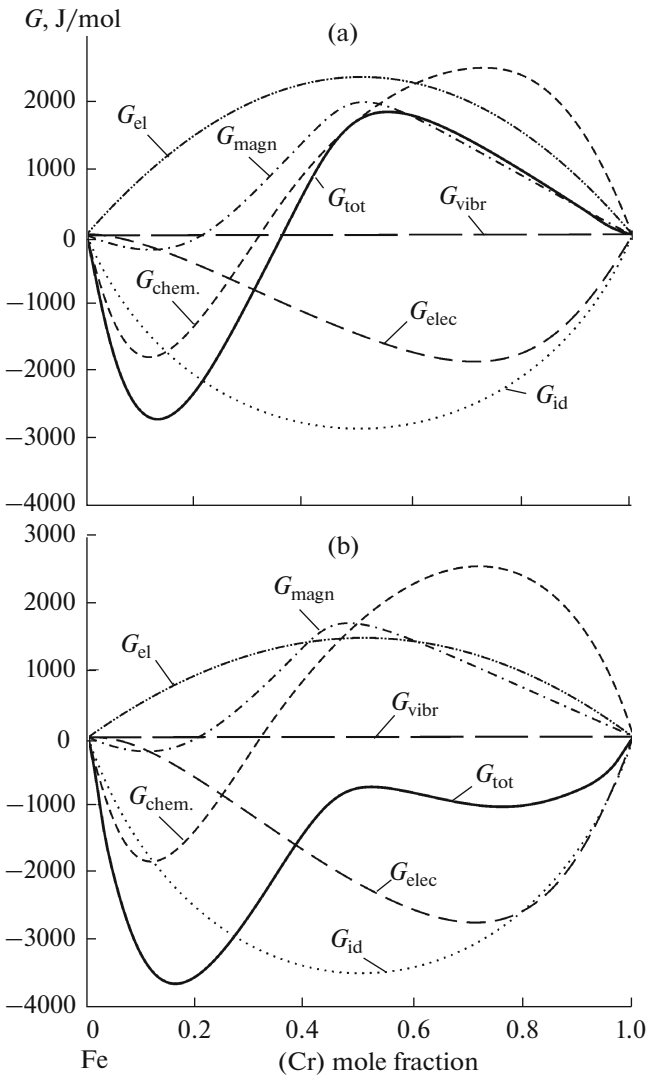

Fig. 1. Calculated energy contributions to Gibbs energy of mixing at T = (a) 500 and (b) 600 K as functions of the solution composition in the Fe–Cr system.

with a fine microstructure, which substantially influence their physical properties [11–28]. These materials should operate at relatively low temperatures, where the operation time does not exceed the diffusion time it takes for phase equilibrium to be reached.

During thermal annealing, either the precipitation of the high-temperature σ phase in an alloy or the phase transformation with the formation of α- and α'-phase precipitates can occur. For example, 2 vol % precipitates form in an Fe–20 at % Cr alloy upon annealing at T = 773 K for 50 h, which inevitably cause local stresses in its crystal lattice [13]. Changes in the structural properties on a microscale can cause significant changes on a macrolevel or, in other words, embrittlement at 475°C; that is, these changes can substantially influence the mechanical properties of the alloy.

The approach described in part I of this work (see [1]) is based on the hypothesis that the free energy of a system (in particular, bcc solid solution) can be expressed as the sum of the following energies of noninteracting subsystems: the energy of chemical interaction during alloy formation at 0 K; the energy of elastic lattice strains caused by the statistical displacements of ionic cores with respect to the sites of an ideal (mean) crystal lattice; the free energy of atomic vibrations in a crystal lattice; the magnetic (or temperature) component of the free energy, which takes into account the contribution of the magnetic subsystem to the heat capacity; the free energy of thermally excited electrons, or the contribution of the electronic component to heat capacity $C_p(x, T)$ at x = const; and the configurational entropy of a random solid solution without regard for short-range order parameters [3, 4]. In [1], we presented the following approximations of the collected experimental data: Debye temperature $\theta_D(x)$, linear thermal expansion coefficients of pure components, which were used to calculate the equilibrium volume of the crystal lattice $V(x, T)$; electronic specific heat coefficients $\Delta\gamma(x)$; average magnetic moment $B_0(x)$; and Curie temperature $\theta_C(x)$. The simulation of the behavior of a material under irradiation is a complex problem, since the processes occurring in this material are nonequilibrium. Various methods are used to simulate the behavior of a material under irradiation. For example, these are ab initio principles, which take into account an electronic structure; molecular dynamics simulation; and the kinetic Monte Carlo method. The last two methods need the knowledge of potentials, which are fitted to the results of ab initio calculations using empirical approaches. This circumstance is a weak point of these two methods, since a reliable theoretical justification of the applied empirical interatomic potentials is now absent. The simulation of equilibrium phase boundaries, which are boundary conditions for nonequilibrium processes, using these two methods requires a huge number of calculations to simulate the motion of a time parameter to infinity. It is difficult to calculate the physical properties, such as the temperature dependence of the isobaric heat capacity of an alloy in both one- and two-phase fields in a phase diagram, using these two methods, since it is necessary to calculate high-order derivatives of the free energy of mixing with respect to alloy composition and temperature.

In principle, the technique proposed in this work can be used to calculate these derivatives, the phase boundaries in a phase diagram, and some physical properties of alloys (bulk modulus, heat capacity, linear thermal expansion coefficient) as functions of the alloy composition and the temperature, which is important in designing new alloys.

PHASE EQUILIBRIUM CALCULATIONS

Figure 1 shows the results of calculating the energy contributions to the Gibbs energy of mixing of ferro-

magnetic bcc solid solutions that were calculated by the formulas from part I of this work at temperatures of 500 and 600 K, since the spinodal changes sharply in this temperature range (Fig. 2). In Fig. 1, the calculated total free energy of mixing G_{tot} as a function of composition (calculation by Eq. (1) from [1]) is shown by the solid line, and the energy contributions (magnetic G_{magn}, vibraitonal G_{vib}, elastic G_{el}, electronic G_{elec}, chemical G_{chem}, and ideal (configurational) G_{id} energies) are shown by the dashed, dotted, and dot-and-dash lines, respectively. As follows from the calculated concentration dependences of the energy contributions, the stabilization of bcc Fe–Cr alloys in the temperature range 500–600 K depends substantially on the elastic, chemical, magnetic, and electronic contributions. As the temperature increases, the influence of the elastic energy caused by the statistical displacements of ionic cores from the sites of the mean crystal lattice weakens, and the influence of the energy of thermally excited electrons strengthens.

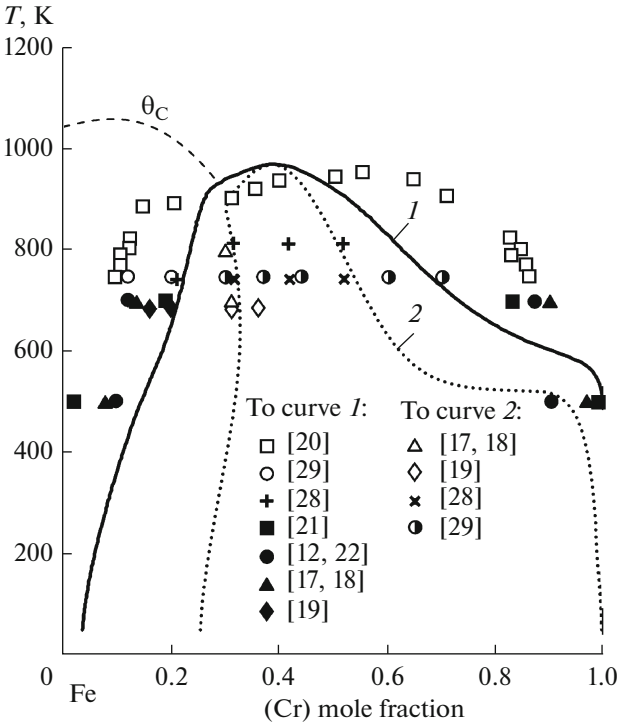

Fig. 2. Calculated curves of (*1*) solubility and (*2*) spinodal of the bcc solid solutions in the Fe–Cr system in comparison with the experimental data (see points).

TECHNIQUE OF THE PHASE EQUILIBRIUM CALCULATIONS

The calculation of phase equilibrium is reduced to the construction of a tangent to the total free energy curve or, in other words, to the Gibbs energy of mixing ${}^{\alpha\alpha}\Delta G^{\alpha}(x, T)$ at a fixed temperature. This is a procedure for searching for the concentration points corresponding to equilibrium phase compositions [14, 15]. According to this procedure, the spinodal points that are the solutions to the equation of zero second derivative of the free energy of mixing with respect to composition are determined to separate roots. The compositions of these phases are then refined at a given accuracy [15]. This procedure is numerically performed because of the complex dependence of the free energy of mixing on the alloy composition and the impossibility of its analytical form.

The second and third derivatives, which are necessary for this procedure, are calculated accurate to the fourth order of expansion $O(h^4)$ using the following formulas [16]:

$$f''_{xx}(x_0) = \frac{-f(x_0+2h)+16f(x_0+h)-30f(x_0)+16f(x_0-h)-f(x-2h)}{12h^2},$$

$$f'''_{xxx}(x_0) = \frac{-f(x_0+3h)+8f(x_0+2h)-13f(x_0+h)+13f(x_0-h)-8f(x_0+2h)+f(x_0-3h)}{8h^3},$$

where f is a function, x_0 is the concentration point where differentiation is performed, and h is the differentiation step. These formulas imply the application of a uniform grid. The necessity of calculation of the third derivative of the free energy of mixing with respect to composition is caused by the determination of the accuracy of calculating spinodal points described by the formula [15]

$$\delta x_{extr} = \delta\left\{\frac{\partial^2 f(x)}{\partial x^2}\right\} \Big/ \left\{\frac{\partial^3 f(x)}{\partial x^3}\right\}\Big|_{x_{extr}}.$$

When performing this procedure in the temperature range 0–1000 K, we found the boundaries of bcc solution solubility and the spinodal line, which are shown in Fig. 2 along with the experimental data obtained in numerous works. The technique of spinodal line calculation is reduced to a numerical differentiation of the mole energy of mixing of the bcc α solution phase ${}^{\alpha\alpha}\Delta G^{\alpha}(x, T)$, which is described with respect to the α phases of the pure components in x (where x is the chromium concentration), and to finding the points of extremum of function $\partial^{\alpha\alpha}\Delta G^{\alpha}(x, T)$.

RESULTS OF THE PHASE EQUILIBRIUM CALCULATIONS

The calculated spinodal line agrees well with the experimental data from [17, 18] for T = 800 K, from

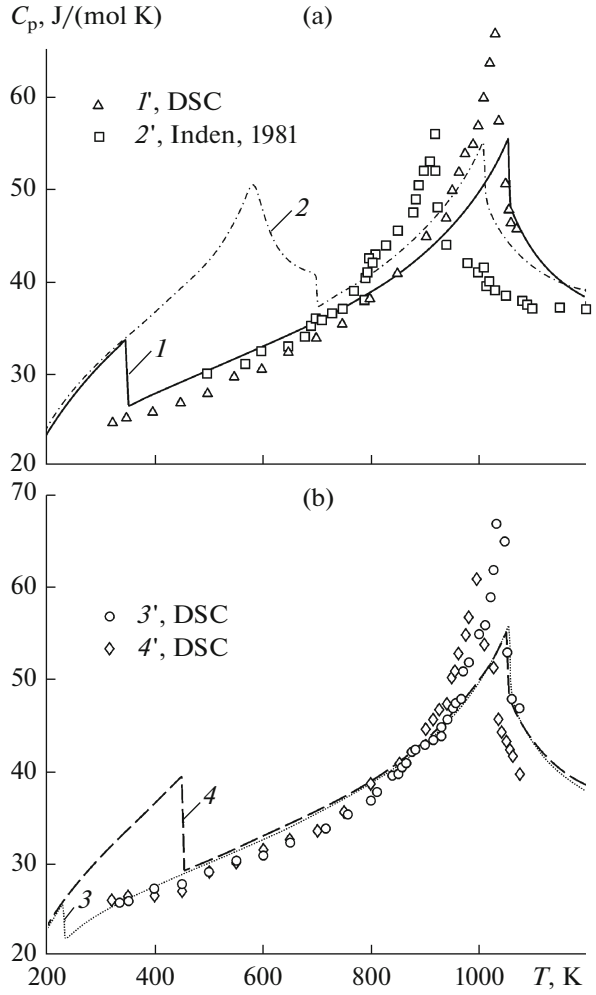

Fig. 3. Calculated isobaric heat capacity of bcc Fe–Cr alloys *1–4* in comparison with the experimental data on the heat capacity of alloys *1'–4'* of the same compositions [17, 18]: (*1*, *1'*) 9.9, (*2*, *2'*) 21.3, (*3*, *3'*) 6.7, and (*4*, *4'*) 13 at % Cr.

[19] for 689 K, and from [28] for 743 K. The visible differences between the calculated solubility boundaries and the values obtained by other researchers, which are seen in Fig. 2, can be explained by the presence of the σ phase, which prevents an exact identification of the α/(α + α') and α'/(α + α') boundaries. As noted in [19], the slow diffusion processes at $T = 700$ K or below can also cause the difference between the experimental and calculated equilibrium solubility boundaries. The coordinates of the calculated critical point are $T_{cr} = 969$ K and $x_{cr}(\mathrm{Cr}) = 0.385$ mole fraction. This point is only of purely theoretical interest, since it belongs to the metastable part of the phase diagram and is "masked" by the phase fields caused by the presence of the σ phase.

The calculated bcc fragment of the Fe–Cr phase diagram is characterized by the prediction of area of solubility of chromium atoms in an iron matrix, which is of particular interest for practice. This area reflects the alternating enthalpy of formation used in the calculations [5–8].

CALCULATION OF THE TEMPERATURE DEPENDENCES OF HEAT CAPACITY

$C_p(T)$ Calculation Procedure

After calculating the equilibrium phase boundaries of bcc solutions, we calculated the temperature dependences of isobaric heat capacities $C_p(T)$ for various alloy compositions. $C_p(T)$ for the two-phase states of the alloys was calculated by the formula [14, 15]

$$C_p^{\alpha+\beta}(x,T) = \alpha(x,T) \times \left(C_p^{\alpha}(x^{\alpha}) + T\left(\frac{\partial x^{\alpha}}{\partial T}\right)^2 \left(\frac{\partial^2 G^{\alpha}}{\partial x^2}\right)_{x^{\alpha}} \right) + \beta(x,T)\left(C_p^{\beta}(x^{\beta}) + T\left(\frac{\partial x^{\beta}}{\partial T}\right)^2 \left(\frac{\partial^2 G^{\beta}}{\partial x^2}\right)_{x^{\beta}} \right),$$

where $\beta = \alpha'$. To describe the slopes of the one- and two-phase boundaries in the phase diagram, we used the van der Waals differential equations

$$\left(\frac{\partial x^{\alpha}}{\partial T}\right)_p = \frac{(G^{\beta})'_T\Big|_{x^{\beta}} - (G^{\alpha})'_T\Big|_{x^{\alpha}} - (G^{\alpha})''_{xT}\Big|_{x^{\alpha}}(x^{\beta} - x^{\alpha})}{(G^{\alpha})''_{xx}\Big|_{x^{\alpha}}(x^{\beta} - x^{\alpha})},$$

$$\left(\frac{\partial x^{\beta}}{\partial T}\right)_p = \frac{(G^{\beta})'_T\Big|_{x^{\beta}} - (G^{\alpha})'_{xT}\Big|_{x^{\alpha}} - (G^{\beta})''_{xT}\Big|_{x^{\beta}}(x^{\beta} - x^{\alpha})}{(G^{\beta})''_{xx}\Big|_{x^{\beta}}(x^{\beta} - x^{\alpha})}.$$

The relation between the $\alpha(x, T)$ and $\beta(x, T)$ phases were determined using the well-known lever rule,

$$\alpha(x,T) = \frac{x - x^{\beta}(T)}{x^{\alpha}(T) - x^{\beta}(T)},$$

$$\beta(x,T) = 1 - \alpha(x,T) = \frac{x^{\alpha}(T) - x}{x^{\alpha}(T) - x^{\beta}(T)}.$$

Results of $C_p(T)$ Calculations

The results of $C_p(T)$ calculations for alloy compositions $x_i(\mathrm{Cr}) = 6.7$, 9.9, 13, and 21 at % are presented in Fig. 3 along with the experimental data from [17, 18]. Note that, depending on temperature, the configuration points of different alloy compositions fall in different fields in the phase diagram, which is reflected on the temperature dependences of heat capacity. First of all, the characteristic λ-type curves are visible. They correspond to the Curie temperatures of alloys of

Calculated and experimental data for the phase boundaries of bcc Fe–Cr alloys at $T = 500$ and 700 K

$T = 600$ K		$T = 700$ K		Investigation technique	Source
x_{Cr}^{α}	$x_{Cr}^{\alpha'}$	x_{Cr}^{α}	$x_{Cr}^{\alpha'}$		
0.03[a]	0.97[a]	0.08[b]	0.89[b]	Estimation from experimental data	[10]
—	—	0.10[c]	0.93[c]	Experiment (Mössbauer spectroscopy)	[20]
0.02[d]	0.99[d]	0.19[b]	0.83[b]	CALPHAD calculation	[21]
—	—	0.08[e]	—	Monte Carlo simulation	[22]
0.08	0.97	0.135[d]	0.9[d]	Quantum-mechanical simulation and CALPHAD calculation	[17]
—	—	0.16–0.19[f]	—	Experiment (annealing, Mössbauer spectroscopy)	[19]
—	—	0.14[g]	0.83[g]	Experiment (annealing, atomic force ionic microscopy)	[24]
0.06–0.09[h]	0.82–0.9[h]	—	—	Experiment (neutron irradiation, AFT)	[25]
—	—	0.17[i]	0.86[i]	Experiment (annealing, AFT)	[26]
—	—		0.92[j]	CALPHAD calculation	[26]
—	—	0.125[k]	—	Experiment (annealing, microhardness)	[27]
—	—	0.2[l]	—	Experiment (calorimetry)	[13]
0.097[m]	0.906[m]	0.12–0.13[m]	0.87[m]	Calculation using concentration-dependent interatomic potentials with allowance for vibrational entropy	[23]
0.145	0.975	0.214	0.732	Calculation with physical–empirical models	This work

(a) Estimation using the data in handbook [10] at 300°C (573 K); (b) at 713 K (invariant equilibrium temperature $\sigma \rightleftarrows \alpha + \alpha'$; (c) obtained in [20] at $T = 673$ K using experimental data obtained by a method based on the Mössbauer effect via calculating the hyperfine magnetic field and the isomer shift for duplex steel (in wt %: 19.9 Cr, 9.98 Ni, 2.42 Mo, 0.69 Mn, 1.2 Si, 0.018 C) annealed at $T = 673$ K for 55 ths h. The authors of [20] stated that diffusion was completed in 22 ths h (result of studying the time evolution of the hyperfine magnetic field); (d) calculated in [17] using the results of quantum-mechanical simulation and CALPHAD calculation; (e) kinetic Monte Carlo method using interatomic potentials, the parameters of which were related to the enthalpy of mixing at 0 K. Electron density functional calculation was performed at 800 K for Fe–Cr alloys containing 12, 15, and 18 at % Cr [22]; (f) obtained in [19] by Mössbauer spectroscopy at $T = 688$ K by calculating the hyperfine magnetic field in a sample annealed for 33 h; (g) obtained in [24] by atomic force microscopy for the Fe–20 at % Cr alloy subjected to annealing at $T = 773$ K for 1067 h; (h) obtained in [25] for neutron irradiation at a dose of 1.82 dpa at $T = 563$ K for model Fe–Cr alloys containing 3, 6, 9, 12, 15, and 18 at % Cr. The irradiated alloys were studied by atomic force tomography (AFT); (i) obtained in [26], where an iron-based oxide-dispersed-strengthened PM 2000™ alloy (in at %: 18.5 Cr, 10.1 Al, 0.58 Ti, 0.17 C, 0.28 O, 0.022 N, 0.228 Y) was studied. The alloy heat treated at $T = 748$ K for 3600 h decomposes into the iron-reach α phase and the aluminum-rich α' phase. The introduction of up to 11 at % Al into the alloy composition was shown to cause aluminum accumulation in the α phase and the suppression of α-phase precipitation; (j) the authors of [26] refer to the calculation of the equilibrium α' phase at $T = 748$ K in the ternary Fe–Cr–Al system that was performed by Scientific Group Thermodata Europe (SGTE); (k) the authors of [27] studied binary and ternary alloys annealed at $T = 748$ K for 1000 h. The diffusion multiple technique was used to accelerate diffusion, and the conclusion regarding the position of the $\alpha/(\alpha + \alpha')$ boundary was drawn from the change in microhardness HV; (l) in [13], C_p of an Fe–20 at % Cr alloy was measured by drop calorimetry. The phase transition $\alpha/(\alpha + \alpha')$ temperature was 702 ± 10 K, and the temperature of the magnetic transition from a para- into a ferromagnetic state was 925 ± 10 K; (m) in [23], the boundaries of solubility of the bcc solid solutions in the Fe–Cr system were calculated for the temperature range 300–1500 K using semiempirical cohesion models with allowance for vibrational entropy.

different compositions at which these alloys transform from a ferromagnetic to a paramagnetic state. As the temperature decreases, the alloys transform from a single-phase to a two-phase state, which is seen as heat capacity jumps in the $C_p(x_i = \text{const}, T)$ curves.

In the temperature range 500–600 K, the temperature dependence of the heat capacity of the alloy with 21 at % Cr in the two-phase state is nonmonotonic, which is caused by a sharp change in the solubility curve of the chromium-rich alloys. This behavior of heat capacity results from the use of the empirical Inden–Hillert–Jarl model, which describes the magnetic contribution to free energy and the influence of the concentration dependence of the Curie temperature on the alloy composition (see Fig. 4 in part I in [1]).

For clarity, we present isothermal sections for the contributions to the free energy of mixing of alloys as functions of the alloy composition at 500 and 600 K (see Fig. 1).

DISCUSSION OF THE CALCULATION RESULTS

Phase Boundaries of the Solubility of bcc Solutions

The results of calculating the boundaries of bcc phase solubility, which are shown in Fig. 2, are compared with the calculated experimental data obtained in other works for temperatures of 500 and 700 K (table).

The physical properties and the solubility boundaries of the system under study were studied by CALPHAD

calculation methods [17, 21], molecular dynamics simulation [12], Monte Carlo simulation [12, 22], experimental Mössbauer spectroscopy [19, 20, 29, 30], isothermal techniques [13, 26], neutron diffraction [25], and quantum-mechanical calculations [5–9]. Complete dissolution of chromium in an iron matrix is predicted in the calculations performed for iron-rich binary alloys with up to 8 at % Cr at room temperature. However, according to the data of all other works, the bcc solution decomposes into pure iron crystallites and pure chromium crystallites at room temperature. The existence of the predicted solid solution in our calculations is caused by the use of the physical model and the results of quantum-mechanical calculations performed in [5, 6] for the first time and then supported in [7, 8]. An alternating run of the concentration dependence of the enthalpy of mixing of bcc solutions at $T = 0$ K was shown in those works.

Temperature Dependences of Iron-Rich Alloys

Figure 3 shows the results of $C_p\{T, x_i(\mathrm{Cr})\}$ calculations along with the experimental data from [17, 18]. The discrepancy between the first high-temperature jumps in the calculated and experimental curves is explained by an insufficiently accurate approximation of the Curie temperature in [1]: a simple approximation function, which described the Curie temperature over the entire concentration range, was chosen to simplify the calculations. Nevertheless, the $C_p(T)$ jumps and the temperature ranges where they occur coincide with the calculated values, which can be considered as a satisfactory result. During motion along the temperature axis from high to low temperatures, the first $C_p(T)$ jumps for the alloys under study correspond to phase transitions through the Curie temperature $\theta_C = 1000–1058$ K, when the alloys pass from a paramagnetic into a ferromagnetic state. The second group of $C_p(T)$ jumps appears when the temperature decreases further and the alloys pass from the single-phase α field to the two-phase $\alpha + \alpha'$ field in the phase diagram. The nonmonotonic behavior of the $C_p(T)$ dependence for the Fe–21 at % Cr alloy in the two-phase field in the phase diagram is caused by specific behavior of the spinodal and corresponds to a sharp change in the spinodal, specifically, its motion from the right boundary of solubility of chromium-rich bcc solutions at $T = 500–700$ K.

Note that it is difficult to experimentally measure the heat capacity jumps during passage through the $\alpha/(\alpha + \alpha')$ phase boundary in the phase diagram at room and moderate temperatures because of a slow diffusion process. Therefore, the results of $C_p(T)$ calculations for various alloy compositions can be recommended to perform experiments on measuring $C_p(T)$ for the alloy compositions and the temperature ranges where equilibrium can be reached within the time intervals that are reasonable and reachable in real experiments.

CONCLUSIONS

Using the results of quantum-mechanical calculations, which predict an alternating run of the concentration dependence of the enthalpy of mixing of bcc solutions at $T = 0$ K, and physical models, we were able to predict the solubility areas of the bcc solutions in iron-rich alloys, namely, at temperatures from room temperature to 750 K for the alloys in a stable state and in the temperature range 750–969 K for the alloys in a metastable state.

The temperature dependences of the heat capacity $C_p(T)$ of Fe–Cr alloys of various compositions in one- and two-phase states were calculated. The calculation results obtained in this work are in good agreement with the experimental and calculated data of other researchers. An analysis of the results of $C_p(T)$ simulation allowed us to develop an experimental technique for testing the existing models and the experimental curve of solubility for iron-rich alloys in the temperature range from room temperature to 475°C. The detected solubility area has not been supported experimentally because of slow diffusion and the long time (several decades) it takes for an equilibrium state in the alloys to be reached.

ACKNOWLEDGMENTS

This work was supported by the Russian Foundation for Basic Research (project nos. 09-03-00983-a, 13-03-00462) and the Department of Chemistry and Materials Sciences of the Russian Academy of Sciences (project OKhNM-02 no. 2013–2015).

REFERENCES

1. A. L. Udovskii and D. A. Vasil'ev, "Application of physical–empirical models to calculate a fragment of the phase diagram and the physical properties of bcc Fe–Cr alloys: I. Formulation of a model and the estimation and approximation of experimental data," Russian Metallurgy (Metally), No. 3, 247–254 (2015).
2. G. Wranglen, *An Introduction to Corrosion and Protection of Metals* (Chapman and Hall, New York, 1985).
3. I. Mirebeau et al., "First measurement of short-range-order inversion as a fraction of concentration in a transition alloy," Phys. Rev. Lett. **53** (7), 687– 690 (1984).
4. I. Mirebeau and G. Parette, "Neutron study of the short-range-order inversion in $\mathrm{Fe}(1 - x)\mathrm{Cr}(x)$," Phys. Rev. B **82**, 104203 (2010).
5. A. A. Mirzoev, M. M. Yalalov, and D. A. Mirzaev, "Calculation of the energy of mixing for the Fe–Cr Alloys by the first-principles methods of computer simulation," Phys. Met. Metallogr. **97** (4), 336–343 (2004).
6. P. Olsson et al., "Ab initio formation energies of Fe–Cr alloys," JNM **321**, 84–90 (2003).

7. P. Olsson et al., "Two-band modeling of α-prime phase formation in Fe–Cr," Phys. Rev. B **72**, 214119 (2005).
8. P. A. Korzhavyi and A. V. Ruban, "Electronic structure and effective chemical and magnetic exchange interactions in bcc Fe–Cr alloys," Phys. Rev. B **79**, 054202 (2009).
9. A. V. Ruban and V. I. Razumovsky, "First-principles based thermodynamic model of phase equilibria in bcc Fe–Cr alloys," Phys. Rev. B **86**, 174111 (2012).
10. O. O. Kubashewski and S. B. Olkokk, *Metallurgical Thermochemistry* (Springer, Berlin, 1979).
11. R. O. Williams and H. W. Paxton, "The nature of aging of binary iron- chromium alloys around 500°C," J. Iron Steel Inst., March, 358–374 (1957).
12. A. Caro, "The computational modeling of alloys: from ab initio and thermodynamics to heterogeneous precipitation," in *Mater. Generat. IV Rectors* (NATO Advanced Study Institute Cargese, 2007), Vol. 6.
13. R. N. Hajra et al., "Thermodynamic stability of Fe–Cr binary system: The crucial role of magnetic contribution as elucidated by calorimetric measurements," Advanc. Mater. Res. **794**, 468–475 (2013).
14. A. L. Udovskii, "Computer simulation of the phase diagrams, the thermodynamic properties, and the structure of multicomponent systems," Izv. Ross. Akad. Nauk, Ser. Met., No. 2, 136–157 (1990).
15. A. L. Udovskii, "Physical fundamentals of computer designing of materials," in *Physical Metallurgy: Manual*, Ed. by B. A. Kalin (MIFI, Moscow, 2012), Vol. 4, Chapter 15.
16. S. C. Chapra and R. P. Canale, *Numerical Methods for Engineers*, 6th Edition (McGraw-Hill, New York, 2010).
17. W. Xiong, P. Hedstrom, M. Selleby, J. Odqvist, M. Thuvander, and Q. Chen, "An improved thermodynamic modeling of the Fe–Cr system down to zero Kelvin coupled with key experiments," CALPHAD **35**, 355–366 (2011).
18. W. Xiong et al., "Phase equilibria and thermodynamic properties in the Fe–Cr system," Critical Rev. Solid State Mater. Sci. **35**, 125–152 (2010).
19. J. Cieslak, S. M. Dubiel, and B. Sepoil, "Messbauer-effect study of phase separation in Fe–Cr system," J. Phys.: Condens. Matter. **12**, 6709–6717 (2000).
20. H. Kuwano and H. Imamasu, "Determination of the chromium concentration of phase decomposition products in an aged duplex stainless steel," Hyperfine Interact. **168** (1–3), 1009–1015 (2006).
21. J. Miettinen, "Thermodynamic reassessment the iron-rich corner," CALPHAD **23** (2), 231 (1999).
22. G. Bonny, D. Terentyev, L. Malerba, and D. van Neck, "Early stages of alpha-alpha-prim phase separation in Fe–Cr alloys: An atomistic study," Phys. Rev. B **79**, 104207 (2009).
23. G. Bonny et al., "Numerical prediction of thermodynamic properties of iron-chromium alloys using semi-empirical cohesive models : The state of the art," J. Nucl. Mater. **385** (2), 268–277 (2009).
24. S. Novy, P. Pareige, and C. Pareige, "Atomic scale analysis and phase separation understanding in a thermally aged Fe–20 at %Cr alloy," J. Nucl. Mater. **384**, 96–102 (2009).
25. M. Bachhav, G. R. Odette, and E. M. Marquis, "α'-Precipitation in neutron-irradiated Fe–Cr alloys," Scripta Materialia **74**, 48–51 (2014).
26. C. Capdevila et al., "Phase separation in PM 2000™ Fe-base ODS alloy: experimental study at the atomic level," Mater. Sci. Eng. A **490**, 277–288 (2008).
27. S. Kobayashi and T. Takasugi, "Mapping of 475°C embrittlement in ferritic Fe–Cr–Al alloys," Scripta Materialia **63**, 1104–1107 (2010).
28. T. de Nys and P. M. Gielen, "Spinodal decomposition in the Fe–Cr system," Met. Trans. **2** (5), 1423–1428 (1971).
29. D. Chandra and L. Schwartz, "Mössbauer effect study on the 475°C decomposition of Fe–Cr," Met. Trans. **2**, 511–519 (1971).
30. Y. Hamaguchi, H. Kuwano, H. Kamide, R. Miura, and T. Yamada, "Effects of proton irradiation on the hardening behavior of HT-9 steel," J. Nucl. Mater. **133–134** (August), 636–639 (1985).

Translated by K. Shakhlevich